DOI: 10.13009/EUCASS2022-6190
9TH EUROPEAN CONFERENCE FOR AERONAUTICS AND SPACE SCIENCES (EUCASS)

Leading Edge Vortex Induced Effects on Electrical Characteristics of a DBD Plasma Actuator

Jannick Erhard, Johannes Kissing* and Jochen Kriegseis***
** Institute of Fluid Mechanics and Aerodynamics (SLA), TU Darmstadt*
Alarich-Weiss-Straße 10, 64287 Darmstadt, Germany
*** Institute of Fluid Mechanics (ISTM), Karlsruhe Institute of Technology (KIT)*
Kaiserstr. 10, 76131 Karlsruhe, Germany
kriegseis@kit.edu

Abstract
On airfoils experiencing unsteady inflow conditions, leading edge vortices (LEV) can be observed. During its growth phase, the LEV has a positive influence on the lift of the airfoil. To extend the growth phase, dielectric barrier discharge plasma actuators are to be used to manipulate the vortex detachment. In order to enable an efficient flow manipulation, the position of the LEV is intended to be used as input to a closed-loop control. Therefore, in the context of the present study, investigations on how the LEV affects the electric characteristics of the plasma actuator are elaborated to ultimately enable the actuator usage simultaneously as a sensor in addition to its flow control task.
First, studies regarding the influence of pressure variation on electrical characteristics are carried out in a vacuum chamber. Subsequently, the influence of the vortex itself on the plasma actuator is investigated on a moving flat plate in a wind tunnel. In both studies, three discharge regimes of the plasma actuator are tested. Measurements in the vacuum chamber show, that the small pressure changes generated solely by the LEV have no significant effect on the electric quantities of the actuator. In contrast, measurements in the wind tunnel indicate, that the LEV has a significant influence on electric characteristics of the actuator in all three discharge regimes. Discrepancies of the results in the vacuum chamber and the wind tunnel are attributed to the flow velocity, which only occurs in the wind tunnel.

1. Introduction

1.1 Background

The leading edge vortex (LEV), which occurs e.g. at plunging and pitching airfoils, is a phenomenon of particular interest for applications in aviation [1,2]. This LEV migrates downstream on the suction side of the wing [3], while providing increased lift as long as it is attached to the leading edge of the wing [4–6]. Due to the formation of further (secondary) vortex structures, the LEV detaches and consequently the lift collapses [7–9]. In order to suppress these secondary structures and expand the growth phase of the LEV to increase the lift, the flow must be actively controlled. For this purpose, dielectric barrier discharge (DBD) plasma actuators (PA) are of interest [10]. The actuator is supplied by a high alternating voltage, which causes a gas discharge. This discharge leads to a so called ionic wind, which results in a directed body force [11,12]. This body force is used to suppress the secondary vortex structures and, thus, the detachment of the LEV can be delayed [13]. DBD PAs are characterized by their low weight and size, which makes them interesting especially for aviation. In addition, high-frequency operation and the absence of mechanical elements, lead to particularly fast response times as required for advanced flow control approaches [14,15].

1.2 Objectives

To operate the actuator in a more efficient way in context of LEV-based lift augmentation, the actuator should be operated in a way that it only suppresses the secondary vortex structures and not hinders the formation of the LEV. Therefore, the device must be switched on and off during the migration of the LEV. Such a close-loop control needs the time-dependent distance of the forming LEV to the actuator as input, which therefore has to be identified. This is problematic, because possible sensors for the determination of the LEV position are constructively difficult to install and/or are disturbed by the electric field of the PA. To overcoming this limit, the overarching goal of the present work

DOI: 10.13009/EUCASS2022-6190

is the application of the PA itself as a sensor for the LEV location, such that the device is able to simultaneously detect the LEV as a sensor and to suppress the secondary vortex structures as an actuator.
The LEV induces a characteristic pressure profile on the suction side of the airfoil, as has been demonstrated in previous studies [16], a pressure minimum was observed on the airfoil below the (travelling) LEV centre position. This pressure profile could be used conversely to detect and track the position of the LEV.
Suitable with these findings, [17,18] were able to demonstrate a direct influence of the pressure on the electrical quantities, especially the current. They showed that a decrease in pressure is accompanied by an increase in the root-mean-square (RMS) of the current, which will be discussed later in more detail. In accordance with the paschens law, [17] additionally shows that the ignition voltage of the actuator decreases with the pressure. However, in the work of [17,18] pressure drops of more than $20\ kPa$ were investigated, while the pressure decrease created by the LEV, according to [16], are just $50 - 200\ Pa$. However, it remains yet to be investigated if the effects found by [17,18] also occur at the lower pressure changes of the LEV, to use this effect for detecting the LEV via its pressure distribution. Therefore – and to furthermore test the measurement setup – investigations in a vacuum chamber are carried out. The LEV not only leads to a decrease in pressure but also to a change in the direction and magnitude of the flow velocity above the airfoil [3]. Studies have shown that the flow velocity, which correlates with the pressure by the Bernoulli's law, also has an influence on the plasma [19,20] and on the metrics of a plasma actuator [21–23]. Consequently, further investigations on a plunging flat plate, creating a LEV, in a wind tunnel are planned.

2. Experimental Method

For the experiments in the pressure chamber a PA is glued onto a perspex plate, as pictured in Figure 1. Copper foil is used for the two electrodes. The exposed electrode has an effective length of 150 mm. To reduce edge effects, the ends of the exposed electrode are rounded and the covered electrode is both longer and wider. 5 layers of Kapton type CMC 70110 are used as dielectric. The AC voltage is applied to the exposed electrode and the covered electrode is grounded. The voltage is provided by a DC voltage source and transformed into a high AC voltage with a Minipulse 2.1 from GBS-Electronics GmbH. To set the required pressure, a Mensor Series 600 automated pressure calibrator is used, which is connected to the pressure chamber via a tube. The pressure chamber is entirely made of perspex.

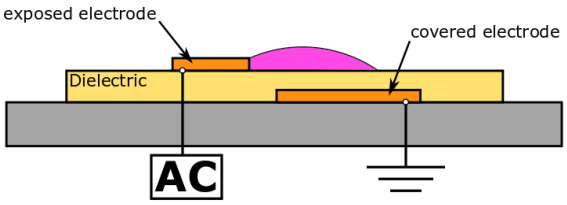

Figure 1: Schematic representation of a considered PA.

The electrical parameters investigated are the voltage drop across the PA $V_{\mathrm{act}}(t)$, the current $I(t)$ and the charge $Q(t)$. In addition, the power of the actuator $P_{\mathrm{act}}(t)$ is used as a measurand. To record the characteristics of the plasma actuator, a Lecroy Wavejet oscilloscope was used with a maximum sample rate of 2 G/s, which can record 500.000 data points per measurement. $V_{\mathrm{act}}(t)$ is tapped across the PA. To determine the current, a resistor of type RNP50S with $R = 1.9994\ \Omega$ is used. The current can be calculated from the voltage drop over the resistor with $I(t) = R \times V_{res}(t)$. If the charge is to be measured, the resistor is replaced by a capacitor of type VISHAV 1813 F0946 with the capacity $C = 21.7$ nF. The charge is calculated using $Q(t) = C \times V_{cond}(t)$. Finally, $P_{\mathrm{act}}(t)$ is determined by the area of the Lissajous figure formed by the voltage $V_{\mathrm{act}}(t)$ and the charge $Q(t)$, as described in [24].
In the pressure chamber, the electric characteristics at different pressures are investigated. The examined pressure differences $\Delta p = \Delta p_{ambient} - p_{chamber}$ are $\Delta p = [0, 10, 50, 75, 100, 150, 200, 500, 1.000]\ Pa$. Also, the PA is operated at different operating points, so called discharge regimes. The first of these discharge regimes is the *darkdischarge*, in which a discharge takes place but no plasma is visible and practically no body force is created. This operating point is considered promising for a control, because here the actuating part of the device is turned off and only the sensing part is active. The second is the *early glowdischarge*, where plasma is visible for the first time. The last operating point studied is the commonly applied regular *glowdischarge* at a peak-to-peak voltage of 12 kV, at which the plasma is fully formed and induces a considerable body force. For this condition it is of interest when the vortex needs to be detected upon actuator active operation.
For the wind tunnel investigations, a plunging and pitching flat plate was used. In this case, a PA is glued onto its surface at 25 % chord length. By means of an actuation a plunging and pitching motion can be performed which leads, as shown in Figure *2*, to the formation of an LEV [13]. The flow velocity in the tunnel is $u_\infty = 2.85\ \mathrm{m/s} \pm 10\ \%$.

DOI: 10.13009/EUCASS2022-6190

The measurement setup used to record the electrical quantities is identical to that used for the pressure chamber. The three discharge regimes described above are also investigated in the wind tunnel. In order to confirm that the effects are caused to the flow mechanical conditions, further comparative measurements are carried out, in which the variables are recorded for a stationary profile at quiescent-air conditions.

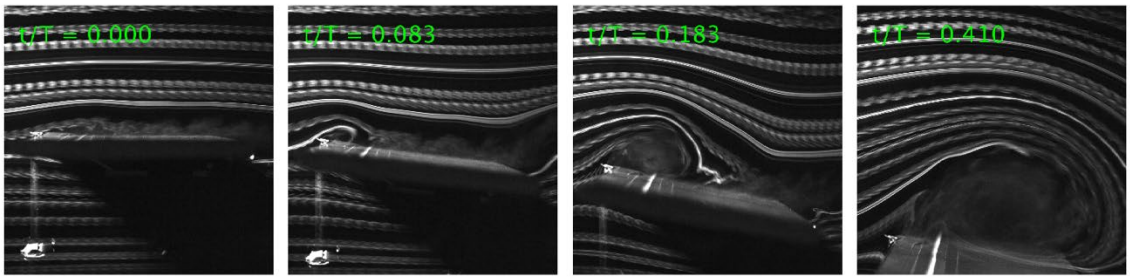

Figure 2: Flow visualization of the LEV-formation on a plunging and pitching flat plate in the wind tunnel.

3. Experimental results

3.1 Pressure Chamber

The following quantities are obtained in the pressure chamber: By smoothing the voltage signal $V_{\mathrm{act}}(t)$, the peak-to-peak voltage V_{pp} is determined, which is then averaged for each measurement. Additionally, as in [17,18], the RMS of the voltage $V_{\mathrm{act}}(t)$, the current $I(t)$, and the charge $Q(t)$, is calculated according to

$$x_{RMS} = \sqrt{\frac{1}{N}\sum_{n=1}^{N}|x_n|^2}, \tag{1}$$

where x is to be replaced by the respectively evaluated quantities in Equation (1) Subsequently, a mean value and a standard deviation were formed from several measurements. Furthermore, for the power $P_{\mathrm{act}}(t)$ of the actuator, the mean value and the standard deviation were also determined. This procedure is applied for each pressure in each studied discharge regime.

Although the experiments in the pressure chamber yielded only a few insights, nevertheless the measuring equipment also used later in the wind tunnel was successfully tested here. It was possible to confirm that the RMS of the current I_{RMS} increases with decreasing pressure, as seen in Figure 3. As in [17,18], this can likewise be attributed to the larger current peaks, shown in Figure 4. However, the pressure changes Δp of 500 Pa and 1000 Pa studied here are significantly higher than those expected by the LEV. The fact, that no significant results were found, can be attributed to some adverse and uncertainty effects. These are the switching behaviour of the plasma actuator, deviations in the manufacturing of the PA, the influence of the plasma ignition on the chamber pressure, and the uncertainty margin of the chamber pressure itself. It can be assumed that the influence of these disturbance variables significantly affects the desired measurement effect such that only trends can be derived from this campaign.

DOI: 10.13009/EUCASS2022-6190

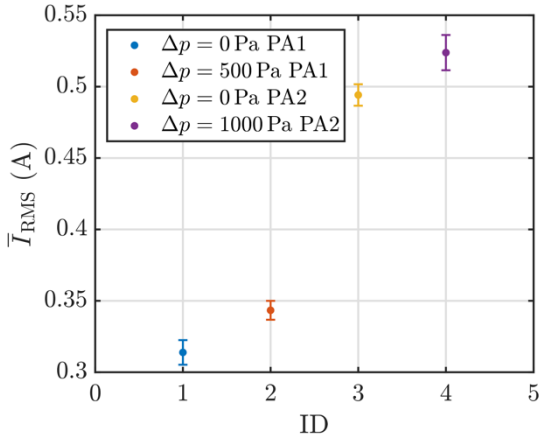

Figure 3: RMS of the current signal at different pressure levels and operating at a peak-to-peak voltage of 12 kV. Different PAs (PA1 & PA2) have been used to avoid the influence of degradation.

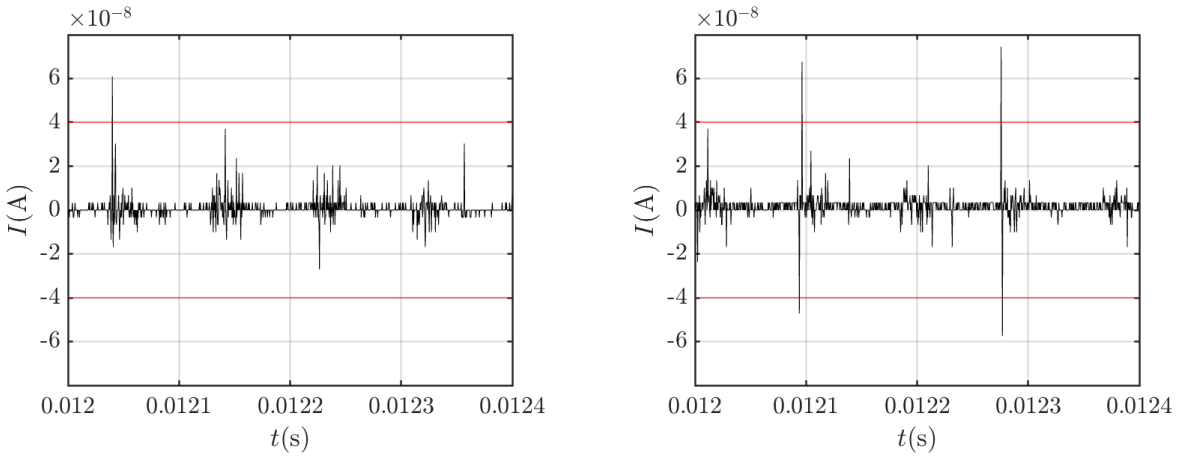

(a) $\Delta p = 0$ Pa (b) $\Delta p = 1000$ Pa

Figure 4: Raw data of the current signal of the PA at different pressure levels and operating at a peak-to-peak voltage of 12 kV. The red lines are for comparison only.

3.2 Wind tunnel

The post-processing carried out for the data of the wind-tunnel investigations differs from that of the pressure chamber in the aspect that now the temporal course of the signals is relevant, since a dynamic system is present here. The conducted data-processing procedure for the tests is exemplarily explained here by means of current signals as obtained in the regime of darkdischarge. The time vector of the signal is normalized to the duration of the full motion period $T = 0.278$ s. The raw data, which can be seen in Figure 5 (a), is smoothed with a moving RMS, leading to I_{RMS}. The RMS window size is 50,001 values and the result of this operation can be seen in Figure 5 (b). All measurements of an ensemble are subsequently normalized to $I_{\mathrm{RMS}}/I_{\mathrm{RMS,sp}}$. In case of the darkdischarge, the I_{RMS} is normalized to its maximum value $I_{\mathrm{RMS,sp}}$ at around $t/T = 0.09$, which corresponds to the moment where the saddle point (SP) of the LEV is above the actuator. A whole ensemble, containing five measurements, is pictured in Figure 5 (c). Note that early and standard glowdischarge instead are normalized to their respective initial values due to the more stable character of these discharge signal histories.
Afterwards, the time-dependent mean value of the ensemble $\bar{I}_{\mathrm{RMS}}/\bar{I}_{\mathrm{RMS,sp}}$ as well as the standard deviation is determined. Here and in the remainder of the manuscript signal standard deviation is indicated as the blue shading; see e.g., Figure 5 (d). In addition, the starting point of the movement t_0 as well as the time at which the LEV is above the plasma actuator t_{LEV} is marked with green and blue vertical lines, respectively. The charge data was treated

DOI: 10.13009/EUCASS2022-6190

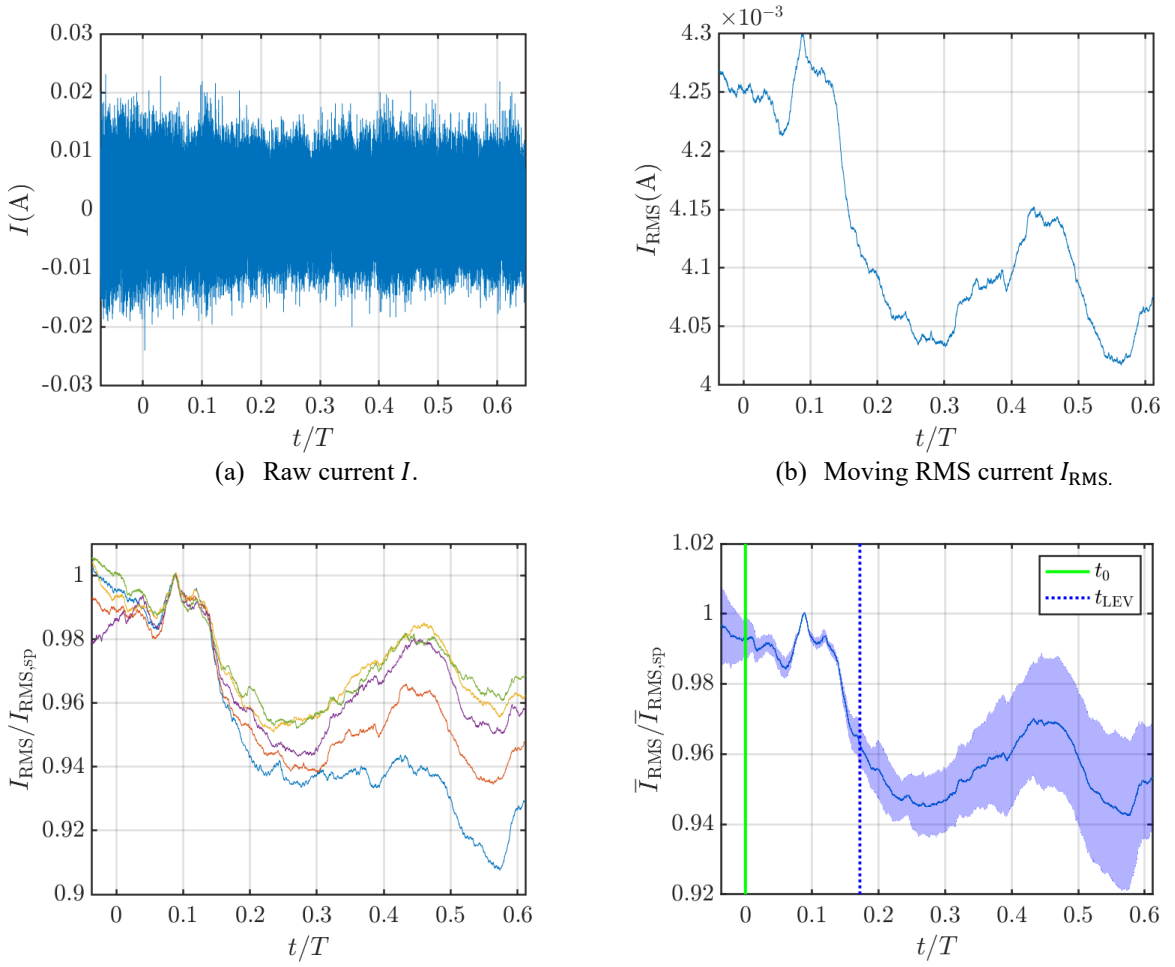

(a) Raw current I.

(b) Moving RMS current I_{RMS}.

(c) $I_{RMS}/I_{RMS,sp}$ for an entire ensemble.

(d) Ensemble average of the RMS current $\bar{I}_{RMS}/\bar{I}_{RMS,sp}$.

Figure 5: Example post-processing of the current measurements of a PA operated in the regime of darkdischarge on a plunging and pitching flat plate.

analogously. Since both the peak-to-peak voltage V_{pp} and the power P_{act} have only positive values, a moving mean with a window size of 501 values is applied here.

The most relevant observations, and meaningful characteristics and/or effects of the electrical parameters are summarized in Table 1, subdivided by discharge regime and parameter. Particularly useful results are highlighted in green.

Table 1: Overview of the effects found, divided by electrical characteristic and discharge regime. The most promising effects are highlighted in green.

Regime	$\bar{V}_{\mathrm{pp,MM}}$	$\bar{I}_{\mathrm{RMS}}$	$\bar{Q}_{\mathrm{RMS}}$	$\bar{P}_{\mathrm{act}}$
Darkdischarge	None significant minimum at t_{LEV}.	Significant decrease of 5 % at t_{LEV}.	No effect.	Some measurements show a maximum at t_{LEV}.
Early glowdischarge	Significant minimum of 0.5 % at t_{LEV}.	None significant maximum at t_{LEV}.	Some measurements show a decrease at t_{LEV}.	Some measurements show a maximum at t_{LEV}.
Glowdischarge ($V_{\mathrm{pp}} = 12$ kV)	Significant minimum of 0.1 % at t_{LEV}.	Significant maximum of 18 % at t_{LEV}.	Decrease of 0.4 % at t_{LEV}.	No effect.

DOI: 10.13009/EUCASS2022-6190

In the darkdischarge regime, a significant effect on the moving RMS current $\bar{I}_{\mathrm{RMS}}$ was found. In Figure *5* (d) can be seen that as the LEV moves across the actuator, the $\bar{I}_{\mathrm{RMS}}$ decreases by 5 %. It is particularly noteworthy that this effect can already be seen in the raw current data. In Figure 6 can be seen that in this case, in contrast to the pressure-chamber results as shown in Figure 3 and Figure 4 or Refs. [17,18], the decrease of $\bar{I}_{\mathrm{RMS}}$ can be contributed to smaller discharge peaks when the vortex is present and the pressure is at its minimum. However, the influences of the tangential velocity must be taken into account here as well as the fact that in the observed regime there is no stable plasma yet. The second decrease appearing at $t/T = 0.45$ can be explained by further smaller vortices following the LEV.

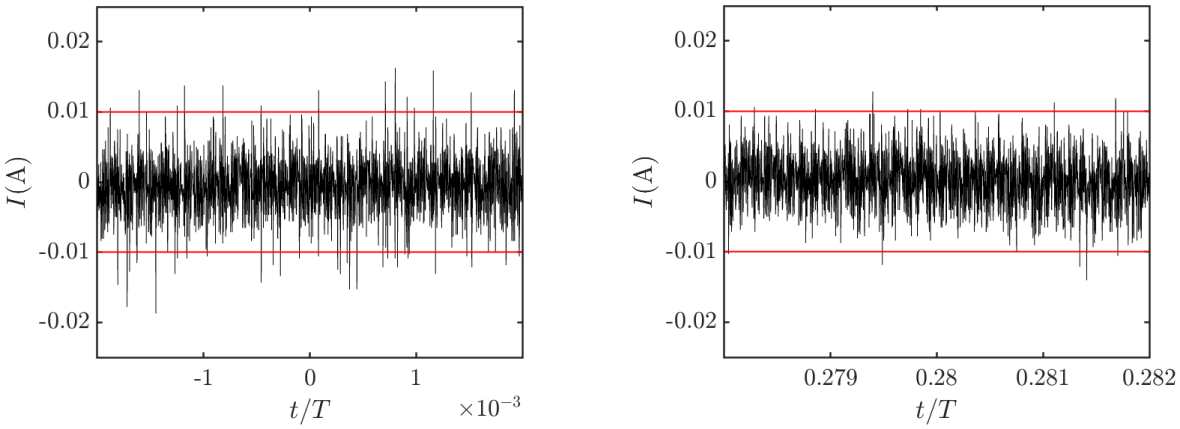

(a) I at t_0. (b) I at $t/T = 0.28$, where $\bar{I}_{\mathrm{RMS}}$ is at its minimum.

Figure 6: Current I of a PA in the regime of darkdischarge at different times of the LEV motion. The red lines are for orientation purposes only.

As shown in Figure *7*, a significant effect on the moving mean of the peak-to-peak voltage $V_{\mathrm{pp,MM}}$ is evident in the early glowdischarge regime. $\bar{V}_{\mathrm{pp,MM}}$ decreases by 0.5 % up to t_{LEV}. As the LEV propagates further, $\bar{V}_{\mathrm{pp,MM}}$ rises again to its initial value. Remarkable, on the one hand, is the small standard deviation and, on the other hand, a second smaller decrease of $\bar{V}_{\mathrm{pp,MM}}$ around $t/T = 0.45$, which again can be explained by smaller vortices following the LEV.

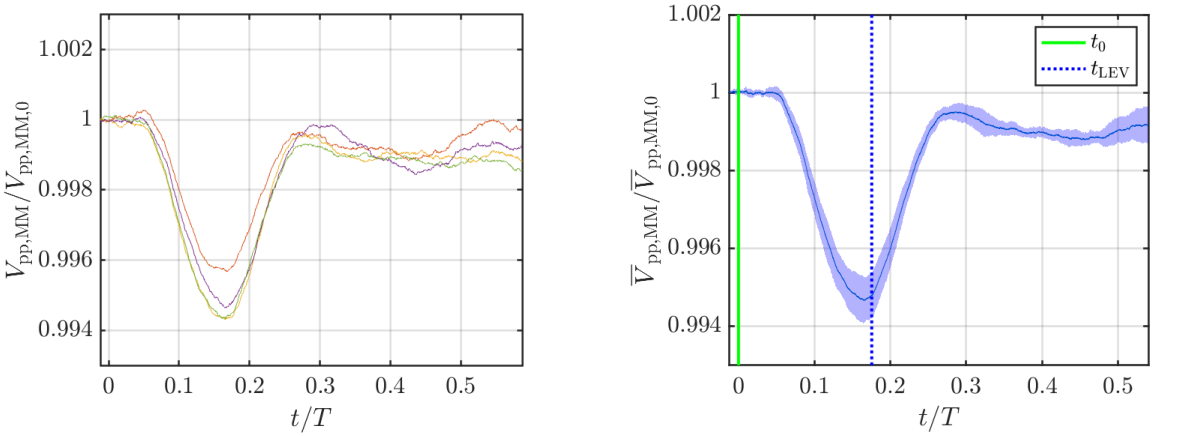

(a) Single measurements of $V_{pp,MM}$. (b) Ensemble average of $V_{pp,MM}$.

Figure 7: Moving mean of V_{pp} of a PA on a plunging and pitching flat plate operated in the regime of early glowdischarge.

Another interesting effect of the vortex motion was observed in the course of the $\bar{I}_{\mathrm{RMS}}$, i.e., several measurements showed an increased RMS value of the current while the vortex center was above the plasma actuator. However, since this effect was not observed in all measurements, it won't be considered further in the following.

DOI: 10.13009/EUCASS2022-6190

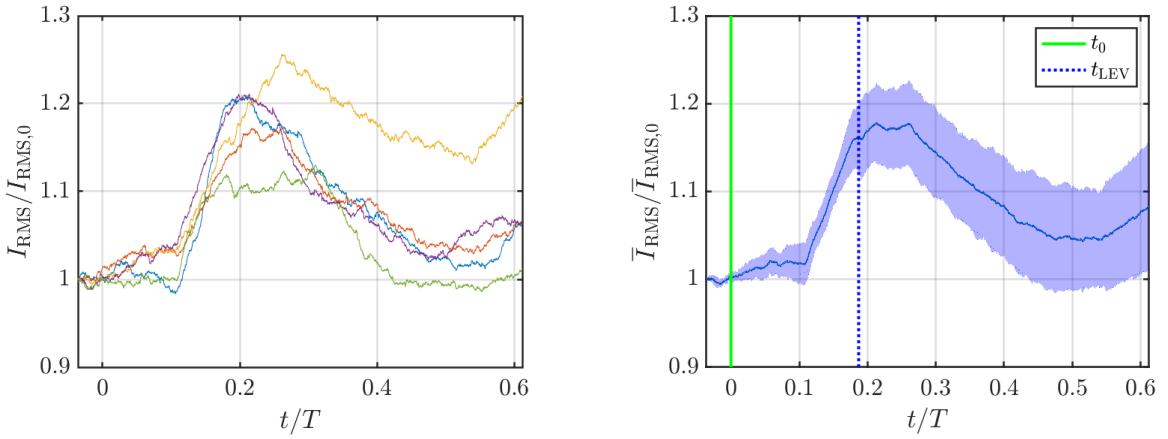

(a) Single measurements of I_{RMS}. (b) Ensemble average of I_{RMS}

Figure 8: Moving I_{RMS} of a PA operated in the regime of glowdischarge at $V_{\mathrm{pp}} = 12$ kV on a plunging and pitching flat plate.

In the third regime studied, the glowdischarge at 12 kV, the effect already found in the early glowdischarge regime was found strongly increased. The moving RMS of the current $\bar{I}_{\mathrm{RMS}}$ increases by 18 % as a result of the approach of the LEV and decreases again as soon as the vortex moves away from the actuator; see Figure 8. When looking at the raw current signal in Figure 9, it can be seen that the current peaks are increasing at the time t_{LEV}. These observations are in agreement with those of the afore-mentioned pressure-chamber results and the observations reported in Refs. [17,18], so that it can be assumed that the pressure minimum of the LEV leads to the observed increase of $\bar{I}_{\mathrm{RMS}}$.

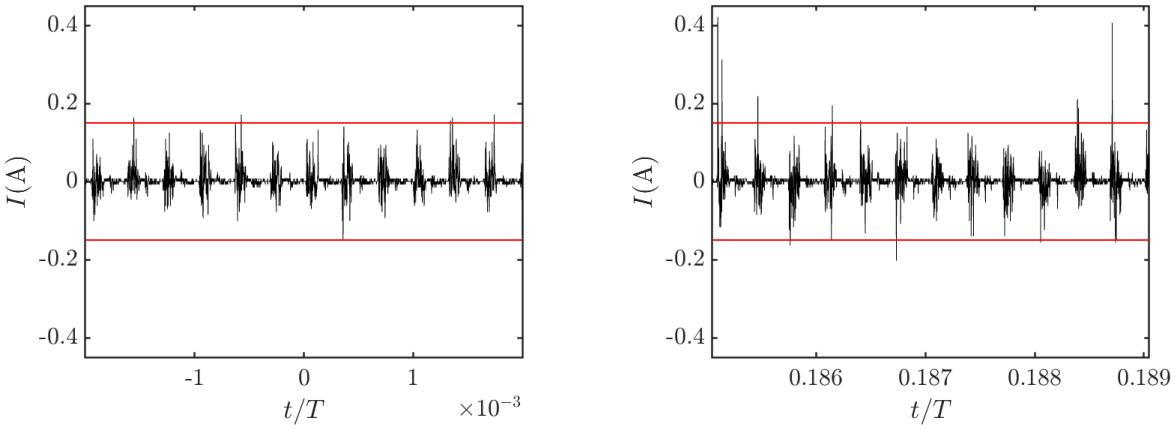

(a) I at t_0. (b) I at t_{LEV}.

Figure 9: I of a PA at 12 kV glowdischarge at different times of the LEV motion. The red lines are for comparison only.

4. Conclusions

In this study the influence of effects induced by the LEV on the electrical characteristics of a dielectric barrier discharge plasma actuator was investigated. The long-term objective is to simultaneously use the PA as a sensor to determine the position of the LEV, while suppressing the formation of secondary vortices as an actuator. Such sensing use of the PA

DOI: 10.13009/EUCASS2022-6190

is expected to provide a real-time, high-frequency control of the actuator, to increase the efficiency of its flow manipulation.
One approach to do so was to use the plasma actuator as a pressure sensor to detect the pressure profile induced by the LEV. This approach seems particularly promising, since several earlier studies have already shown some effects of the pressure on the electrical quantities of the plasma actuator. The major challenge of the presented work was the evaluation of whether these effects are also observable for the much smaller pressure changes induced by the LEV. To investigate this effect, first a vacuum chamber was used. Different pressure levels and discharge regimes of the plasma actuator were tested, where only trends were extractable regarding vortex detection have been revealed.
To appraise the influence of the vortex itself on the electrical quantities of the plasma actuator, experiments in a wind tunnel with a moving flat plate were carried out. In this case also the influence of the flow velocity at and on the PA have to be considered. Again, different types of discharge of the plasma actuator were investigated. In this latter campaign, some noteworthy effects in all three discharge regimes were found: In the dark discharge regime, where no plasma is visible, a strong decrease in the RMS of the current at the transition of the vortex was observable. In the regime of early glowdischarge, when plasma first becomes visible at the actuator, a minimum in the peak-to-peak voltage was found at the time when the vortex centre was above the plasma actuator. In the third investigated regime of glowdischarge at 12 kV peak-to-peak voltage, the vortex transition was accompanied by a sharp increase in RMS current.
In continuation of the present work, future investigations are foreseen to relate the effects found here to the position of the LEV in order to use this information as an additional input for closed loop control of the DBD PA.

References

[1] C.P. Ellington, The novel aerodynamics of insect flight: applications to micro-air vehicles, The Journal of experimental biology 202 (1999) 3439–3448.
[2] S.J. Newman, Principles of Helicopter Aerodynamics – Second edition J.G. Leishmann Cambridge University Press, The Edinburgh Building, Shaftesbury Road, Cambridge, CB2 2RU, UK. 2006. 826pp. Illustrated. £65. ISBN 0-521-85860-7, Aeronaut. j. 111 (2007) 825–826.
[3] J. Kissing, J. Kriegseis, Z. Li, L. Feng, J. Hussong, C. Tropea, Insights into leading edge vortex formation and detachment on a pitching and plunging flat plate, Exp Fluids 61 (2020).
[4] C.P. Ellington, C. van den Berg, A.P. Willmott, A.L.R. Thomas, Leading-edge vortices in insect flight, Nature 384 (1996) 626–630.
[5] J.R. Usherwood, C.P. Ellington, The aerodynamics of revolving wings I. Model hawkmoth wings, The Journal of experimental biology 205 (2002) 1547–1564.
[6] C.W. Pitt Ford, H. Babinsky, Lift and the leading-edge vortex, J. Fluid Mech. 720 (2013) 280–313.
[7] D.E. Rival, J. Kriegseis, P. Schaub, A. Widmann, C. Tropea, Characteristic length scales for vortex detachment on plunging profiles with varying leading-edge geometry, Exp Fluids 55 (2014).
[8] J. Kissing, S. Wegt, S. Jakirlic, J. Kriegseis, J. Hussong, C. Tropea, Leading edge vortex formation and detachment on a flat plate undergoing simultaneous pitching and plunging motion: Experimental and computational study, International Journal of Heat and Fluid Flow 86 (2020) 108726.
[9] J. Kissing, J. Kriegseis, C. Tropea, On the Role of Secondary Structures During Leading Edge Vortex Lift Off and Detachment on a Pitching and Plunging Flat Plate, in: A. Dillmann, G. Heller, E. Krämer, C. Wagner, C. Tropea, S. Jakirlić (Eds.), New Results in Numerical and Experimental Fluid Mechanics XII, Springer International Publishing, Cham, 2020, pp. 204–213.
[10] J. Kriegseis, B. Simon, S. Grundmann, Towards In-Flight Applications? A Review on Dielectric Barrier Discharge-Based Boundary-Layer Control, Applied Mechanics Reviews 68 (2016).
[11] C.L. Enloe, T.E. McLaughlin, R.D. VanDyken, K.D. Kachner, E.J. Jumper, T.C. Corke, Mechanisms and Responses of a Single Dielectric Barrier Plasma Actuator: Plasma Morphology, AIAA Journal 42 (2004) 589–594.
[12] E. Moreau, Airflow control by non-thermal plasma actuators, J. Phys. D: Appl. Phys. 40 (2007) 605–636.
[13] J. Kissing, B. Stumpf, J. Kriegseis, J. Hussong, C. Tropea, Delaying leading edge vortex detachment by plasma flow control at topologically critical locations, Phys. Rev. Fluids 6 (2021).
[14] L.N. Cattafesta, M. Sheplak, Actuators for Active Flow Control, Annu. Rev. Fluid Mech. 43 (2011) 247–272.
[15] Thomas C. Corke, Benjamin Mertz, Mehul P. Patel, Plasma Folw Control Optimized Airfoil, 44th AIAA Aerospace Sciences Meeting and Exhibit (2006).
[16] A. Eslam Panah, J.M. Akkala, J.H.J. Buchholz, Vorticity transport and the leading-edge vortex of a plunging airfoil, Exp Fluids 56 (2015).
[17] Benjamin J. Chartier, An Investigation on the Application of DBD Plasma Actuators as Pressure Sensors, AIAA Aerospace Sciences Meeting (2009).
[18] M.M. Hollick, M. Arjomandi, B.S. Cazzolato, An investigation into the sensory application of DBD plasma actuators for pressure measurement, Sensors and Actuators A: Physical 171 (2011) 102–108.

DOI: 10.13009/EUCASS2022-6190

[19]F.C. Lindvall, A glow discharge anemometer, Electr. Eng. 53 (1934) 1068–1073.
[20]R.F. Mettler, The anemometric application of an electrical glow discharge in transverse air streams, 1949.
[21]J. Kriegseis, S. Grundmann, C. Tropea, Airflow influence on the discharge performance of dielectric barrier discharge plasma actuators, Physics of Plasmas 19 (2012) 73509.
[22]R. Pereira, D. Ragni, M. Kotsonis, Effect of external flow velocity on momentum transfer of dielectric barrier discharge plasma actuators, Journal of Applied Physics 116 (2014) 103301.
[23]J. Kriegseis, K. Barckmann, J. Frey, C. Tropea, S. Grundmann, Competition between pressure effects and airflow influence for the performance of plasma actuators, Physics of Plasmas 21 (2014) 53511.
[24]J. Kriegseis, B. Möller, S. Grundmann, C. Tropea, Capacitance and power consumption quantification of dielectric barrier discharge (DBD) plasma actuators, Journal of Electrostatics 69 (2011) 302–312.